Article

Cell

Broadly Neutralizing Antibody 8ANC195 Recognizes Closed and Open States of HIV-1 Env

Graphical Abstract

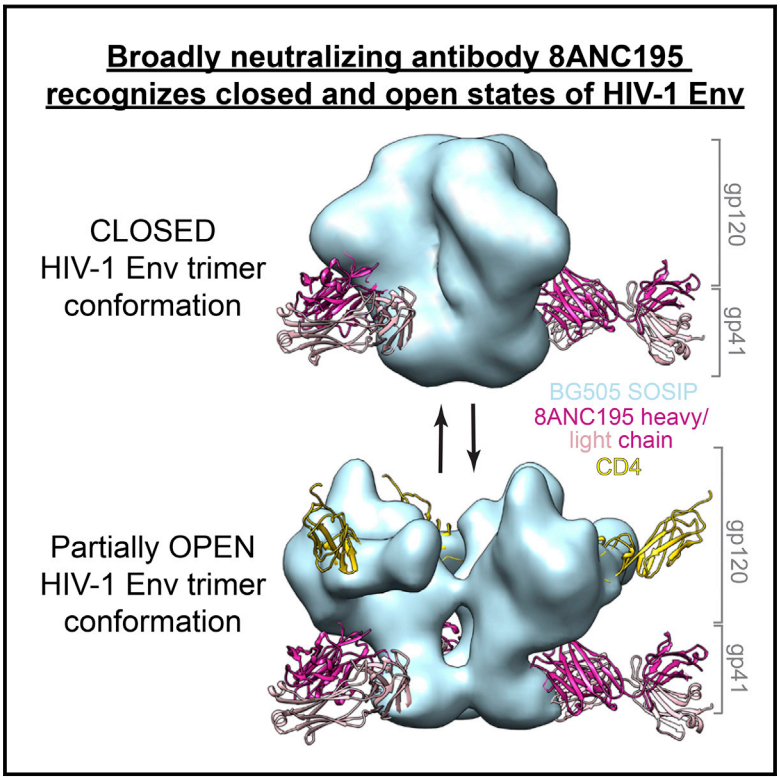

Authors

Louise Scharf, Haoqing Wang, Han Gao, Songye Chen, Alasdair W. McDowall, Pamela J. Bjorkman

Correspondence

bjorkman@caltech.edu

In Brief

Broadly neutralizing antibodies against the HIV-1 viral envelope are under consideration for therapeutic administration to prevent or treat infection. Structural analysis of one such antibody not only uncovers a previously unseen conformation of the envelope, but also marks a new site of virus vulnerability.

Highlights

- 3.58 Å structure of 8ANC195-Env trimer defines the gp120-gp41 site of HIV vulnerability
- EM structure shows 8ANC195 binds Env trimer in CD4-bound partially open state
- 8ANC195 partially reverses CD4-induced open Env conformation
- Binding closed and open Env suggests neutralization of free and cell-bound virus

Accession Numbers

5CJX

Scharf et al., 2015, Cell *162*, 1–12
September 10, 2015
http://dx.doi.org/10.1016/j.cell.2015.08.035

CellPress

Please cite this article in press as: Scharf et al., Broadly Neutralizing Antibody 8ANC195 Recognizes Closed and Open States of HIV-1 Env, Cell (2015), http://dx.doi.org/10.1016/j.cell.2015.08.035

Article

Cell

Broadly Neutralizing Antibody 8ANC195 Recognizes Closed and Open States of HIV-1 Env

Louise Scharf,[1] Haoqing Wang,[1] Han Gao,[1] Songye Chen,[1] Alasdair W. McDowall,[1,2] and Pamela J. Bjorkman[1,*]
[1]Division of Biology and Biological Engineering, California Institute of Technology, Pasadena, CA 91125, USA
[2]Howard Hughes Medical Institute, California Institute of Technology, Pasadena, CA 91125, USA
*Correspondence: bjorkman@caltech.edu
http://dx.doi.org/10.1016/j.cell.2015.08.035

SUMMARY

The HIV-1 envelope (Env) spike contains limited epitopes for broadly neutralizing antibodies (bNAbs); thus, most neutralizing antibodies are strain specific. The 8ANC195 epitope, defined by crystal and electron microscopy (EM) structures of bNAb 8ANC195 complexed with monomeric gp120 and trimeric Env, respectively, spans the gp120 and gp41 Env subunits. To investigate 8ANC195's gp41 epitope at higher resolution, we solved a 3.58 Å crystal structure of 8ANC195 complexed with fully glycosylated Env trimer, revealing 8ANC195 insertion into a glycan shield gap to contact gp120 and gp41 glycans and protein residues. To determine whether 8ANC195 recognizes the CD4-bound open Env conformation that leads to co-receptor binding and fusion, one of several known conformations of virion-associated Env, we solved EM structures of an Env/CD4/CD4-induced antibody/8ANC195 complex. 8ANC195 binding partially closed the CD4-bound trimer, confirming structural plasticity of Env by revealing a previously unseen conformation. 8ANC195's ability to bind different Env conformations suggests advantages for potential therapeutic applications.

INTRODUCTION

The envelope (Env) spike of HIV-1, a trimer of gp120-gp41 heterodimers, is the only target of neutralizing antibodies (Abs) and therefore the focus of vaccine design efforts. The discovery of highly potent broadly neutralizing antibodies (bNAbs) isolated from a subset of HIV-1-infected donors has brought new impetus to the idea of delivering bNAbs passively to protect against or treat HIV-1 infection. bNAbs have been shown to prevent and treat infection in mouse and macaque models (reviewed in West et al., 2014) and exhibited efficacy against HIV-1 in a human clinical trial (Caskey et al., 2015). Defining the epitopes and neutralization mechanisms of anti-HIV-1 bNAbs provides critical information for selecting combinations of bNAbs for passive delivery efforts and for design of immunogens to elicit similar Abs in a vaccine and can illuminate the complex process of viral entry.

Until recently, the HIV-1 Env spike was considered to have four defined bNAb epitopes: three on the gp120 subunit (the V1V2-glycan epitope at the apex of the Env trimer, the V3-loop region centered on the $Asn332_{gp120}$ oligomannose patch, and the binding site for the host receptor CD4) and the fourth involving the gp41 membrane-proximal external region (MPER) (reviewed in West et al., 2014). Within the last year, three Abs were discovered to target distinct regions of the gp120-gp41 interface. Two of the subunit-spanning bNAbs, PGT151 and 35O22, are trimer specific and do not bind to gp120 monomers (Blattner et al., 2014; Huang et al., 2014). The gp120-gp41-spanning bNAb 8ANC195 binds both to gp120 monomers and gp140 trimers (Scharf et al., 2014; Scheid et al., 2011).

8ANC195 was originally isolated in a screen that identified many CD4-binding site (CD4bs) Abs, but its epitope did not map as a conventional CD4bs bNAb (Scheid et al., 2011). We used computational analyses of neutralization data to predict that intact potential *N*-linked glycosylation sites at positions 234_{gp120} and 276_{gp120} are essential for the activity of 8ANC195, suggesting that the epitope was near, but not within, the CD4bs on gp120 (West et al., 2013). A 3.0 Å resolution crystal structure of 8ANC195 Fab and CD4 domains 1 and 2 (sCD4) bound to a gp120 core revealed extensive contacts with *N*-linked glycans attached to $Asn234_{gp120}$ and $Asn276_{gp120}$ and defined a site of Env vulnerability involving glycans and the gp120 inner domain that is not targeted by other bNAbs (Scharf et al., 2014). Finally, negative-stain single-particle electron microscopy (EM) reconstruction of a native-like soluble Env trimer (BG505 SOSIP.664, hereafter referred to as BG505 SOSIP [Sanders et al., 2013]) complexed with three 8ANC195 Fabs confirmed the binding site on gp120 and further suggested that 8ANC195 spanned the gp120-gp41 subunit interface to contact gp120 with its heavy chain (HC) and gp41 with its light chain (LC) (Scharf et al., 2014). These structural studies suggested that 8ANC195 did not inhibit HIV-1 infection by blocking the CD4bs on gp120 (indeed, the crystal structure demonstrated simultaneous binding of sCD4 and 8ANC195 Fab) but, rather, that recognition of both Env subunits by 8ANC195 could facilitate neutralization by preventing conformational changes required for gp41-mediated fusion of the host cell and viral membranes.

However, the precise nature of the 8ANC195 epitope on gp41 could not be elucidated due to the low resolution of the 8ANC195-BG505 SOSIP EM structure; nor was it known whether 8ANC195 would block or accommodate conformational changes in Env trimers upon CD4 binding. To address these

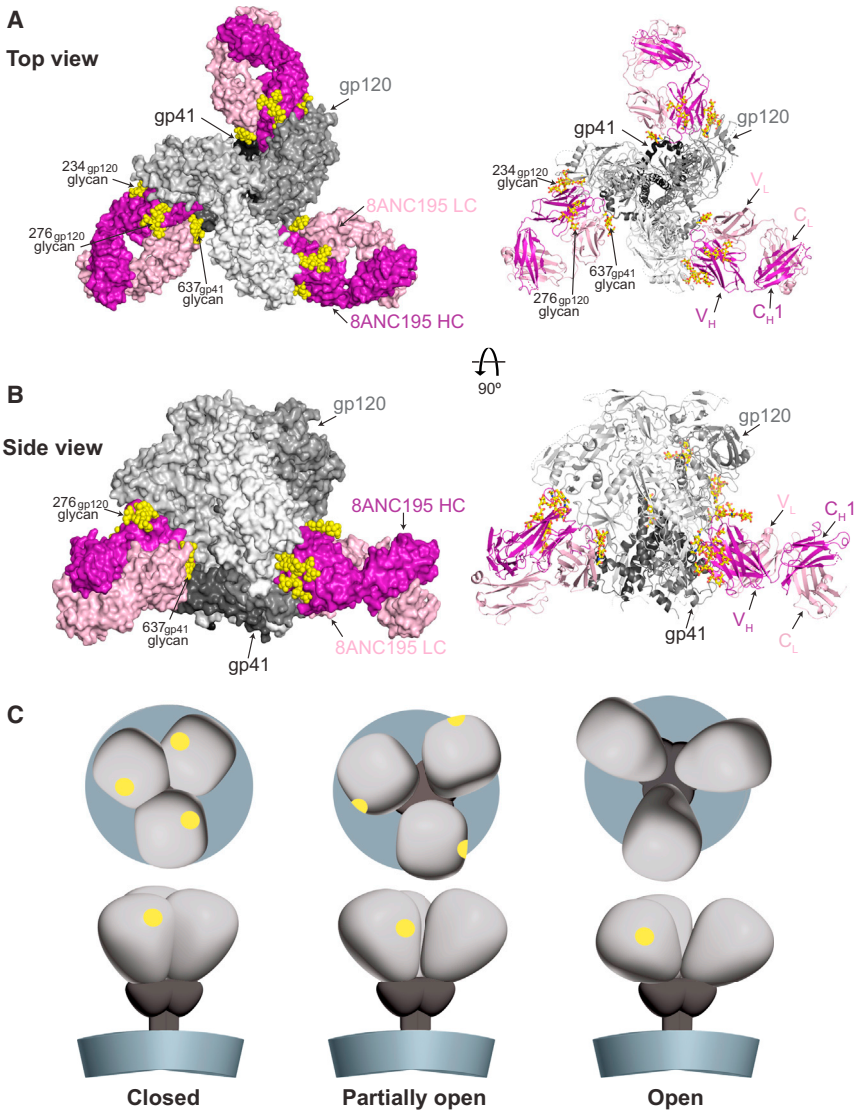

Figure 1. Overview of 8ANC195$_{G52K5}$-BG505 SOSIP Structure

8ANC195$_{G52K5}$ Fabs are dark pink (HC) and light pink (LC), gp120 subunits are different shades of light gray, and gp41 subunits are different shades of dark gray. *N*-linked glycans at the Fab-trimer interface are yellow.

(A) 8ANC195$_{G52K5}$-Env structure seen from the top in space-filling (left) and ribbon diagram (right) representations.

(B) 8ANC195$_{G52K5}$-Env structure seen from the side in space-filling (left) and ribbon diagram (right) representations.

(C) Conformations of HIV-1 Env trimers shown schematically (adapted from figures in Liu et al., 2008) as seen from above (top) and the side (bottom) (CD4-binding site, yellow; remainder of gp120, light gray; gp41, dark gray; membrane, blue-gray). The closed structure was observed for unliganded virion-bound trimers (Liu et al., 2008) and structures involving liganded BG505 SOSIP trimers (Julien et al., 2013a; Lyumkis et al., 2013; Pancera et al., 2014). The partially open structure was observed for virion-bound trimers associated with b12 or A12 (Liu et al., 2008). Open structures were observed for trimers associated with CD4 or the Fab from the CD4-induced Ab 17b (Merk and Subramaniam, 2013).

See also Figure S1 and Table S1.

questions, we solved a crystal structure of an 8ANC195-BG505 SOSIP complex to define the 8ANC195 epitope at the gp120-gp41 interface at atomic resolution, allowing structural comparison of a subunit-spanning bNAb bound to a gp120 monomer and to a gp140 Env trimer. Furthermore, we used binding studies to show that 8ANC195 can recognize CD4-bound Env trimers; thus, the conformational changes induced by CD4 binding do not preclude 8ANC195 recognition of the gp120-gp41 interface. To visualize the conformational state of Env trimer bound to both CD4 and 8ANC195, we used three-dimensional (3D) EM reconstruction to demonstrate that 8ANC195 binding prevents the full opening of Env trimer that is associated with the conformational change induced by CD4 to allow subsequent co-receptor binding and fusion of host and viral membranes. These studies provide structural and biochemical evidence of a bNAb recognizing both the closed and open conformational states of HIV-1 Env and suggest that the ability to accommodate conformational change on its target antigen benefits an anti-HIV-1 bNAb.

RESULTS

Characterization of Complete 8ANC195 Epitope in the Context of HIV-1 Env Trimer

To elucidate the complete 8ANC195 epitope on Env trimer at atomic resolution, we solved a 3.58 Å resolution crystal structure of a more potent 8ANC195 variant, $\gamma52_{HC}\kappa5_{LC}$ (Scharf et al., 2014) (hereafter referred to as 8ANC195$_{G52K5}$), complexed with BG505 SOSIP (Figure 1 and Table S1). Trimers were expressed in kifunensine-treated HEK cells to yield protein containing $Man_{8-9}GlcNAc_2$ high-mannose *N*-glycans (Elbein et al., 1990) at all potential *N*-linked glycosylation sites (pseudoviruses containing only high-mannose glycans or mixtures of high-mannose and complex glycans were neutralized equivalently by 8ANC195$_{G52K5}$; Table S3). Crystallization trials were conducted with complexes of BG505 SOSIP, sCD4, and 8ANC195$_{G52K5}$ Fab produced by first purifying BG505 SOSIP complexed with sCD4 by size exclusion chromatography (SEC) (Figures S1A and S1B), adding 8ANC195$_{G52K5}$ Fab, and then repeating the SEC to purify the ternary complex (Figure S1C). Although the crystallization drops contained all three proteins, resulting crystals did not include sCD4 (Figure S1D), and electron density maps showed density only for one BG505 SOSIP and three 8ANC195$_{G52K5}$ Fabs per asymmetric unit. When we docked

three copies of sCD4 in the appropriate location on BG505 SOSIP by aligning the gp120-sCD4 portion of the 8ANC195-gp120-sCD4 complex structure (PDB: 4P9H) with gp120 in the trimer portion of 8ANC195$_{G52K5}$-BG505 SOSIP structure and refined their all-atom occupancies, the occupancies of sCD4 atoms refined toward zero, confirming the absence of sub-stoichiometric amounts of sCD4 in the crystals.

The 8ANC195$_{G52K5}$-BG505 SOSIP structure revealed the variable heavy (V_H), variable light (V_L), and constant heavy and light (C_H1 and C_L) domains of three Fabs bound at the gp120-gp41 interface of an Env trimer (Figures 1A and 1B). The trimer is in the closed, prefusion state, similar to the conformation of BG505 SOSIP in previous crystal and EM structures (Julien et al., 2013a; Do Kwon et al., 2015; Lyumkis et al., 2013; Pancera et al., 2014) and as revealed for bNAb-bound BG505 SOSIP by hydrogen-deuterium exchange (Guttman et al., 2015), rather than the open conformation observed in EM structures of both virion-associated and soluble Env trimers, including sCD4 or the CD4-induced Ab 17b (Harris et al., 2011; Liu et al., 2008; Sanders et al., 2013; Tran et al., 2012) (Figure 1C). Since no Abs were bound to the apex of the trimer in our crystals, by contrast with previous crystal structures of BG505 SOSIP bound to PGT122 (Julien et al., 2013a) or PGT122 and 35O22 (Pancera et al., 2014), the V1/V2 loops of the trimer in the 8ANC195$_{G52K5}$-BG505 SOSIP structure are less ordered (Figure S1E). However, well-resolved regions of the trimer showed no major structural rearrangements compared with a previous structure of similar resolution (PDB: 4TVP) (Figure S1E). Trimers for previous crystal structures contained only high-mannose *N*-linked glycans that were treated with EndoH to truncate accessible *N*-linked glycans to a single *N*-acetyl glucosamine (NAG) (Julien et al., 2013a; Do Kwon et al., 2015; Pancera et al., 2014), whereas our trimer structure includes all potential *N*-linked glycans in an untruncated form. Nevertheless, we observed no major conformational changes compared with previous structures, with the exception of some disordering of the trimer apex, likely due to the lack of stabilization by crystal contacts or Fab binding to this region.

The placement of the 8ANC195$_{G52K5}$ V_H domain relative to the gp120 subunit of gp140 was relatively close to that observed in the 8ANC195-gp120-sCD4 complex structure (Cα rmsd of 2.1 Å; all V_H residues), with closest agreement at the 8ANC195$_{G52K5}$-gp120 interface (Figure S2A). The interactions with gp120 are reproduced in the context of the trimer, including contacts with protein residues in the gp120 inner domain and with *N*-linked glycans at Asn234$_{gp120}$ and Asn276$_{gp120}$ (Figures 2A, 2B, and 3 and Table S2). The Asn276$_{gp120}$ glycan, normally complex type in native HIV-1 Envs (Binley et al., 2010; Go et al., 2011), is high mannose in the crystallized Env trimer. This gp120 glycan forms an interface with framework region residues in V_H domain strands A and B and the N-terminal portion of CDRH1 using only the core pentasaccharide common to both high-mannose and complex-type *N*-glycans (Scharf et al., 2014), which we suggested is an adaptation to recognize both complex-type and high-mannose glycans at a particular *N*-linked glycosylation site on Env (Mouquet et al., 2012; Scharf et al., 2014). The overall conformation of V_H is conserved (Cα rmsd of 0.67 Å after aligning all V_H residues). However, there are rearrangements in the residues of the third complementarity determining region of the HC (CDRH3) to accommodate and interact with gp41 (Figures 2B, 3, S2C, and S2D). Furthermore, V_L is shifted slightly from the position observed in the 8ANC195-gp120-sCD4 structure, also to accommodate and interact with gp41 (Figures 2B, 3, S2C, and S2D). Compared with the low-resolution EM reconstruction (Scharf et al., 2014), the 8ANC195$_{G52K5}$-BG505 SOSIP crystal structure shows a closer interaction of the Fab and trimer, confirming the Fab placement observed in the complex structure with gp120 (Figure S2E).

As described previously, 8ANC195 contacts a large epitope on gp120 alone (3,750 Å^2 of total buried surface area in gp120-8ANC195-sCD4 structure [Scharf et al., 2014]). The epitope on gp120 is 3,835 Å^2 in the context of the trimer (Figures 2A and 2B and Table S2), and contacts with gp41 make the 8ANC195$_{G52K5}$ epitope more extensive, adding 1,810 Å^2 total buried surface area between gp41 and the Fab (485 Å^2 between gp41 and HC; 1,325 Å^2 between gp41 and LC). 771 Å^2 of this interface is between the LC and the Asn637$_{gp41}$ glycan, which is ordered to the branching mannose (MAN) residue in the core pentasaccharide (NAG-NAG-MAN) (Figures 2C and 3). The first CDR of the LC, CDRL1, stabilizes CDRH3 and interacts with residues near the kink in α9$_{gp41}$ (nomenclature for gp41 secondary structures as in Pancera et al., 2014) and residues 613$_{gp41}$–615$_{gp41}$ in a loop N terminal to α8$_{gp41}$ that is positioned underneath the kink in α9$_{gp41}$ at Asn637$_{gp41}$ (Figures 2C and 3). This interaction rationalizes our previous observation that a germline (gl) reversion that altered two residues and removed one from CDRL1 (T30S$_{LC}$, G30aΔ_{LC}, N31S$_{LC}$) drastically decreased the potency of 8ANC195 (Scharf et al., 2014), possibly because Gly30a$_{LC}$ introduces a kink in CDRL1 that allows the mature Ab to engage and accommodate this region of gp41. The second LC CDR, CDRL2, mainly accommodates the Asn637$_{gp41}$ glycan (Figure 2C). A conservative two-residue gl reversion in this loop (G51A$_{LC}$, A52S$_{LC}$) caused a large decrease in neutralization potency (Scharf et al., 2014), likely because the loop in the mature Ab containing Gly51$_{LC}$-Ala52$_{LC}$ is more compact and flexible, allowing the LC to avoid clashes with the Asn637$_{gp41}$ glycan. Thr30$_{LC}$ is within hydrogen-bonding distance of Glu634$_{gp41}$ and Ser615$_{gp41}$ side chains and the backbone carbonyl oxygen of Tyr638$_{LC}$. Other LC residues in CDRL1 and CDRL2 in the vicinity of gp41 could participate in water-mediated H bonds (Asn31$_{LC}$, Trp32$_{LC}$, Arg50$_{LC}$, Gly51$_{LC}$, and Leu54$_{LC}$), but we cannot place water molecules at the current resolution.

To determine the functional importance of gp41 contacts by 8ANC195, we assessed the effects of alanine mutants of 8ANC195 HC and LC residues located in the vicinity of gp41 in the 8ANC195$_{G52K5}$-BG505 SOSIP structure (Table S3 and Figure 3). 8ANC195 IgG mutants W32A$_{LC}$, Y49A$_{LC}$, and Y91A$_{LC}$ showed decreased neutralization potencies against HIV-1 strains YU2 and BG505, and W100aA$_{HC}$ showed slightly decreased potency against YU2 (Table S3). These results are rationalized by the complex structure (Figure 3): Trp100a$_{HC}$, conserved in all 8ANC195-related HCs (Scharf et al., 2014), inserts its side chain into a hydrophobic pocket at the gp120-gp41 interface, suggesting that the loss of this interaction reduces the binding energy. The W32A$_{LC}$ mutation resulted in a complete loss of neutralization potency against YU2 and BG505. Trp32$_{LC}$ makes no direct contacts with gp41 but could

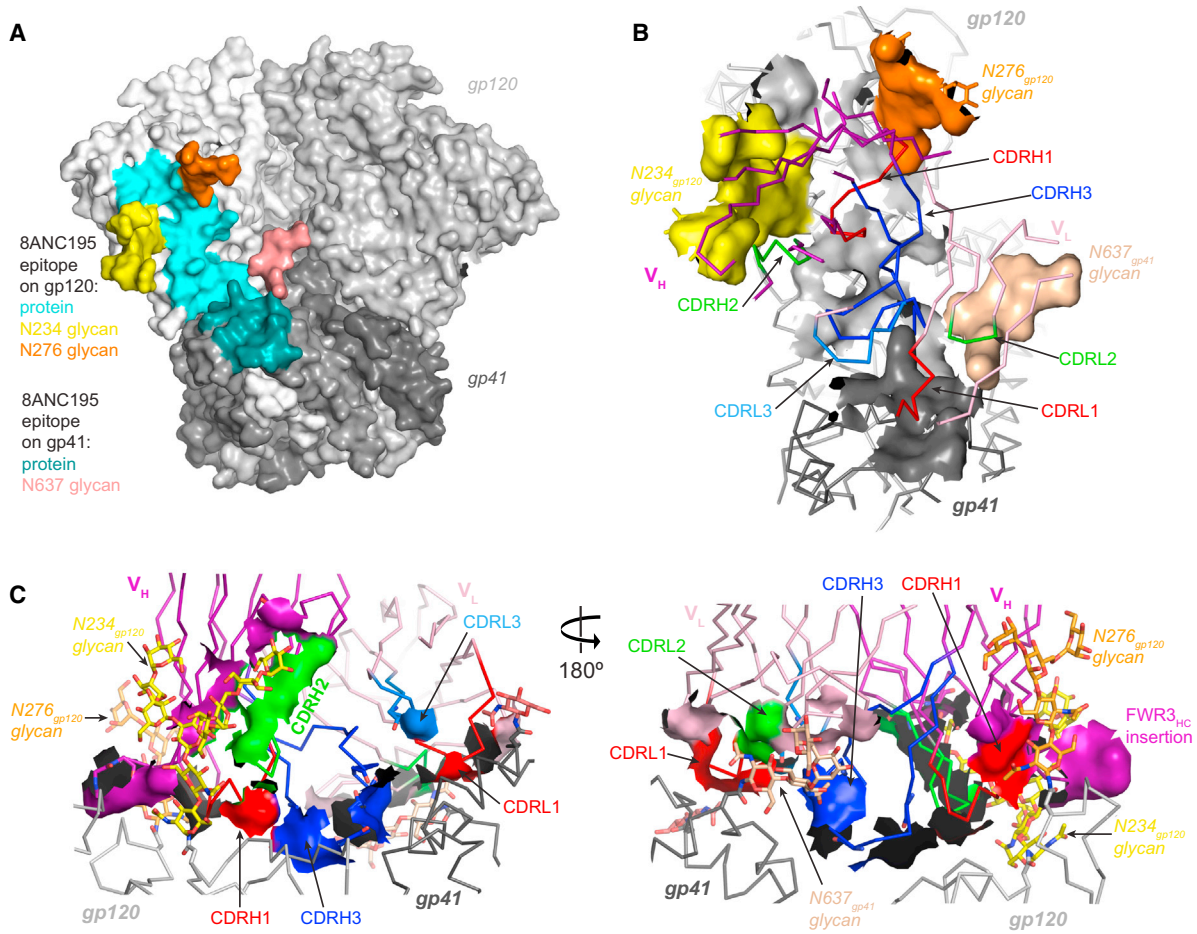

Figure 2. Interfaces in 8ANC195$_{G52K5}$-BG505 SOSIP Structure

(A) 8ANC195$_{G52K5}$ epitope. BG505 SOSIP is shown in space-filling representation with the gp120 and gp41 portions of one protomer in white and medium gray, respectively (other two protomers are light gray). Glycan and protein portions of the 8ANC195$_{G52K5}$ epitope are highlighted in the indicated colors on one protomer.

(B) Close-up of contact areas. Relevant portions of 8ANC195$_{G52K5}$ are shown in wire representation with atoms within buried surface areas on BG505 SOSIP shown as colored surfaces.

(C) Details of interactions with glycans on gp120 and gp41. Buried surface areas on 8ANC195$_{G52K5}$ are shown as colored surfaces.

See also Figure S2 and Table S2.

engage in water-mediated H bonds with Glu634$_{gp41}$. In addition, it makes stacking interactions with His100f$_{HC}$ side chain, likely stabilizing the complicated CDRH3 conformation involved in gp120 interactions (Scharf et al., 2014). The hydroxyl group of Tyr49$_{LC}$ is within hydrogen-bonding distance of the branching mannose of the Asn637$_{gp41}$ glycan, potentially allowing the Ab to accommodate this conserved glycan, and the ring portion of the side chain makes hydrophobic interactions with Leu100d$_{HC}$, potentially stabilizing the CDRH3 conformation. The hydroxyl group of Tyr91$_{LC}$ forms H bonds with Gly100c$_{HC}$ and Lys50$_{LC}$, again stabilizing the CDRH3 conformation.

Effects of *N*-Linked Glycans Attached to gp41 on Neutralization by 8ANC195

To further explore the roles of *N*-linked glycans within the 8ANC195 epitope on gp41, we evaluated the effects of removing glycans attached to Asn611$_{gp41}$, Asn625$_{gp41}$, and Asn637$_{gp41}$ (by one, two, or three Asn-Gln mutations) on YU2 pseudovirus neutralization by WT 8ANC195 and partially gl-reverted chimeric Abs.

Neutralization by 8ANC195 did not depend strongly upon the presence of glycans attached to Asn611$_{gp41}$, Asn625$_{gp41}$, or Asn637$_{gp41}$ (Table S4). However, glycan recognition may play a more prominent role during maturation of 8ANC195 from its gl progenitor, as evidenced by neutralization behaviors of partial gl chimeric LCs. 8ANC195 containing a gl reversion that altered two residues and removed one from CRDL1 (T30S$_{LC}$, G30aΔ$_{LC}$, N31S$_{LC}$) (8ANC195 glCDRL1) exhibited >130-fold reduced neutralization potency against YU2 compared to the fully mature Ab, but its neutralization capacity was completely ablated if the Env target lacked glycosylation at Asn611$_{gp41}$ or Asn625$_{gp41}$. These glycans may have partially stabilized Ab binding in

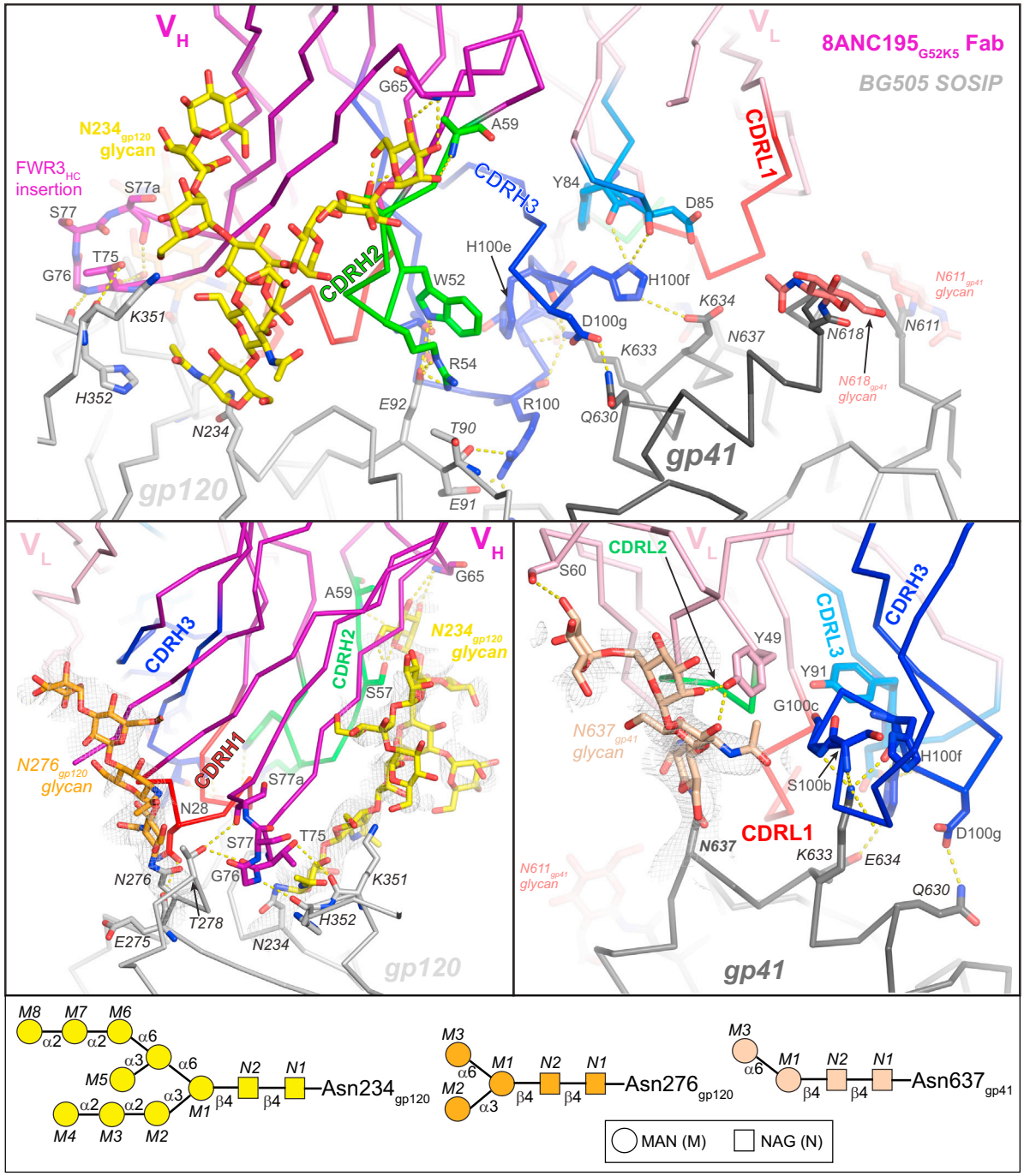

Figure 3. Contacts between 8ANC195$_{G52K5}$ Fab and BG505 SOSIP Protein Residues and Glycans

Proteins are shown as Cα traces with interface residues as sticks (oxygen, red; nitrogen, blue). CDRs and framework regions (FWRs) of 8ANC195$_{G52K5}$ at the interface are highlighted and labeled. Putative H bonds are shown as yellow dots. Env glycans at the interface are yellow (Asn234$_{gp120}$), orange (Asn276$_{gp120}$), and tan (Asn637$_{gp41}$) and are enclosed in electron density from a 2F$_o$-F$_c$ simulated annealing omit map contoured at 1.0 σ (gray mesh) in the lower structure panels. Schematic structures of the ordered portions of these *N*-linked glycans are shown at the bottom.

See also Tables S3 and S4.

progenitors of the mature 8ANC195, which would have had shortened CDRL1 loops in addition to two amino acid substitutions. Conversely, glycosylation at Asn637$_{gp41}$ may destabilize binding of progenitor Abs since neutralization potency of 8ANC195 glCDRL1 against YU2 was partially restored (16-fold) when the Asn637$_{gp41}$ site was knocked out. The destabilizing

A

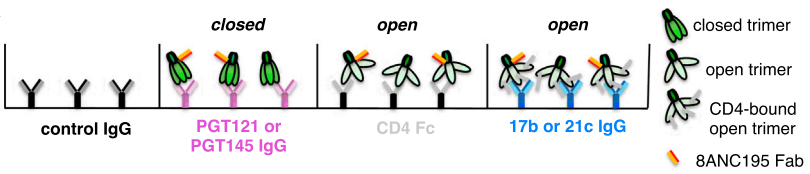

B

Capture protein / Fab analyte	K_D (nM) PGT145 IgG	PGT121 IgG	CD4-Fc	17b IgG	21c IgG
8ANC195	86 ± 18	47 ± 8	133 ± 19	N.D.	N.D.
$8ANC195_{G52K5}$	40 ± 13	33 ± 10	89 ± 4	39 ± 29	42 ± 26
G52HC/8ANC195LC	47 ± 18	23 ± 8	82 ± 7	N.D.	N.D.

Figure 4. Effects of Env Trimer Conformational State on Binding Affinity of 8ANC195

(A) Schematic representation of coupled surfaces and injected analytes. A control IgG (mG053), an IgG recognizing closed trimers (PGT121 or PGT145), CD4-Fc (recognizing open trimers), and a CD4-induced Ab (17b or 21c) recognizing open CD4-bound trimers were immobilized on separate flow cells of a biosensor chip. BG505 SOSIP trimers were injected, resulting in binding to surfaces except for the control flow cell. 8ANC195, $8ANC195_{G52K5}$, or a $G52_{HC}/8ANC195_{LC}$ chimera Fab was then injected over the IgG-BG505 SOSIP complex.

(B) Summary of affinities (K_D values; reported as mean ± SD for three independent experiments) for combinations of capture proteins and analytes. Since PGT145 indirectly inhibited binding of 8ANC195 to BG505 SOSIP trimers and PGT121 enhanced 8ANC195 binding (Derking et al., 2015), our affinity measurements likely underestimated (PGT145-captured trimers) or overestimated (PGT121-captured trimers) the affinity of 8ANC195 for closed trimer. N.D., not determined.

See also Figure S3.

influence of $Asn637_{gp41}$ glycosylation had a greater effect than stabilizing influences of $Asn611_{gp41}$ and $Asn625_{gp41}$ glycans, as the net effect in double or triple knockouts involving $Asn637_{gp41}$ was only partial restoration of neutralizing activity. In the case of a target with an $Asn611_{gp41}/Asn637_{gp41}$ double knockout, neutralization by 8ANC195 glCDRL1 was improved by >30-fold and was brought to within the same order of magnitude as mature 8ANC195.

8ANC195 containing a conservative two-residue gl reversion in CDRL2 ($G51A_{LC}$, $A52S_{LC}$) (8ANC195 glCDRL2) was ~16-fold reduced in neutralization potency compared to the mature Ab; its remaining potency was further diminished by 8.6-fold if the YU2 Env lacked glycosylation at $Asn625_{gp41}$ but was partially restored (1.8-fold) if it lacked glycosylation at $Asn637_{gp41}$. The restorative effect of the knockout of $Asn637_{gp41}$-linked glycosylation was again dominant over effects of also removing $Asn625_{gp41}$-linked glycan in a double knockout. The knockout of $Asn611_{gp41}$-linked glycosylation had only a minor effect on neutralization by 8ANC195 glCDRL2 but amplified the restorative effect of the $Asn637_{gp41}$ knockout from 1.8-fold to >8-fold in the double and triple knockouts. The CDRL2 loop lies in apposition to the glycan attached to $Asn637_{gp41}$ in the $8ANC195_{G52K5}$-BG505 SOSIP crystal structure and ~15 Å from the $Asn611_{gp41}$ glycosylation site (Figure 3). Given the closer proximity of CDRL2 to the $Asn637_{gp41}$ glycan, interactions between the two might be influenced synergistically by a loss of glycosylation at $Asn611_{gp41}$. In the case of a chimeric Ab containing the mature 8ANC195 HC and a gl LC (8ANC195 mHC/glLC), which had a 19-fold reduced neutralization potency against YU2, a stabilizing effect of $Asn611_{gp41}$ glycosylation and destabilizing effect of $Asn637_{gp41}$ glycosylation were evident in several of the pairings.

These results are consistent with $Asn637_{gp41}$ glycosylation interfering with neutralization of a partially immature 8ANC195, $Asn625_{gp41}$ glycosylation enhancing neutralization, and $Asn611_{gp41}$ glycosylation having positive or detrimental effects depending on complex factors. Mature 8ANC195 may have evolved promiscuity toward recognition of viruses, including the presence or absence of glycans at these positions, which may be present in a viral swarm containing many mutated viruses, perhaps through layers of redundancy in stabilizing interactions that are only revealed on partial reversion to the gl form. Thus, we speculate that mature 8ANC195 accommodates, rather than productively interacts with, at least some of the gp41 glycans.

8ANC195 Binds CD4-Bound Env Trimers

We previously showed that 8ANC195 and sCD4 can bind simultaneously to monomeric gp120 and that addition of sCD4 did not detectably alter the in vitro neutralization potency of 8ANC195 (Scharf et al., 2014). sCD4 binding has little to no effect on the structures of monomeric gp120 cores (Kwon et al., 2012) but results in rotation of gp120 protomers to create an open structure in virion-bound Env trimers and SOSIP gp140s, including BG505 SOSIP (Harris et al., 2011; Liu et al., 2008; Sanders et al., 2013; Tran et al., 2012) (Figure 1C). Although sCD4 does not preclude binding of 8ANC195 to gp120, changes between the closed and open states of trimeric Env at the gp120-gp41 interface could disrupt the 8ANC195 epitope on open Env trimers.

To determine whether 8ANC195 can bind sCD4-bound open Env trimers, we used SPR to evaluate binding to different trimer conformational states. For these experiments, we immobilized IgGs on a biosensor chip that captured BG505 SOSIP trimers with different bNAbs: PGT145 and PGT121, which bind to closed Env (Julien et al., 2013a; Pancera et al., 2014; Pugach et al., 2015); CD4-Fc (Capon et al., 1989), which should capture open trimers; and CD4-induced Abs 17b and 21c (Sullivan et al., 1998; Xiang et al., 2002), which should capture sCD4-bound open trimers (Figures 4A and S3). 17b Fab induces opening of some Env trimers in the absence of CD4 binding (Tran et al.,

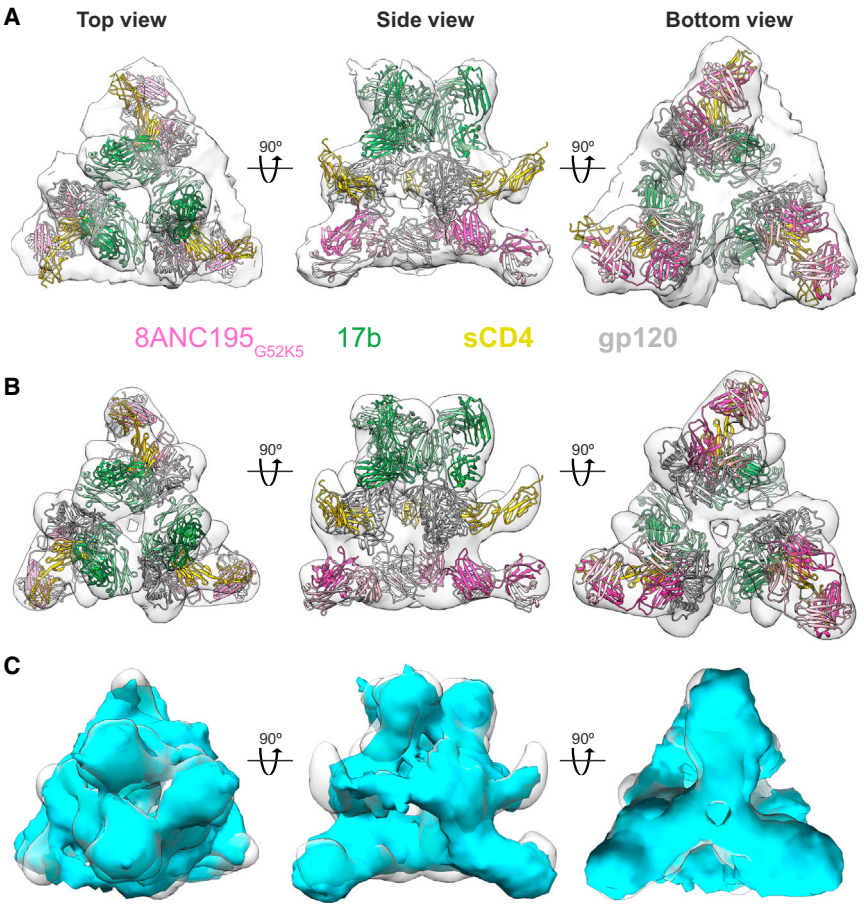

Figure 5. EM Reconstructions of BG505 SOSIP-sCD4-17b-8ANC195$_{G52K5}$ Complex

The X-ray structures of a gp120-scD4-17b complex (PDB: 1RZK) and 8ANC195 Fab (PDB: 4P9M) were fit to EM densities and are shown from the top, side, and bottom.

(A) ~23 Å resolution EM density derived from cryo-ET and sub-tomogram averaging.

(B) ~17 Å resolution EM density derived from negative-stain single-particle reconstruction.

(C) Superposition of densities from cryo-ET/sub-tomogram averaging (cyan) and negative-stain single-particle (light gray) reconstructions.

See also Figures S4 and S5.

8ANC195 Recognizes a Partially Open Env Trimer in the Presence of sCD4 and 17b

Having shown that it is possible for 8ANC195/8ANC195$_{G52K5}$ to recognize CD4-bound BG505 SOSIP trimers, we sought to determine how this class of Ab accommodates conformational changes involved in transitioning from the closed to open trimeric state (Figure 1C). We prepared complexes of BG505 SOSIP trimers—sCD4, 17b Fab, and 8ANC195$_{G52K5}$ Fab—for EM structure determinations (Figures 5, 6, S4, and S5), reasoning that binding of 17b Fab to a CD4-bound open trimer would prevent a potential full reversion to a closed trimeric conformation since it is not possible to accommodate three 17b Fabs at the apex of a closed gp140 trimer (Figure 6A). To ensure that the trimers were in an open conformation when given the opportunity to bind 8ANC195$_{G52K5}$, we first purified BG505 SOSIP-sCD4-17b complexes by SEC, added 8ANC195$_{G52K5}$ Fab, and then subjected the four-component mixture to SEC again, obtaining stable quaternary complexes, as confirmed by SDS-PAGE (Figure S4A).

In order to obtain a reference-free reconstruction of the BG505 SOSIP-sCD4-17b-8ANC195$_{G52K5}$ complex that included no assumptions about trimer conformation or how many ligands were bound, we initially determined a ~23 Å structure by sub-tomogram averaging of cryoelectron tomography (cryo-ET) data obtained from 3D reconstruction of a tilt series of two-dimensional (2D) projection images (Figures 5A and S4). With no model or symmetry imposed, the sub-tomogram-averaged structure showed a 3-fold symmetric particle with densities for three 17b Fabs at the apex, three sCD4 molecules around the middle, and three 8ANC195$_{G52K5}$ Fabs at the bottom. Since a co-crystal structure of gp120-sCD4-17b can be fit as a unit into EM structures of open CD4-bound Env trimers (Harris et al., 2011; Liu et al., 2008; Sanders et al., 2013), we first fit the density with gp120-sCD4-17b coordinates (PDB: 1RZK), resulting in a 3-fold symmetric distribution of gp120, sCD4, and 17b. We next fit 8ANC195 Fab (PDB: 4P9M) into three protruding densities at the predicted gp120-gp41-spanning epitope.

2012), but 17b does not bind to BG505 SOSIP unless sCD4 is present (Sanders et al., 2013), and the 21c epitope includes portions of CD4 as well as gp120 (Diskin et al., 2010). Thus, both CD4-induced Abs will only bind to sCD4-BG505 SOSIP complexes.

8ANC195 and 8ANC195$_{G52K5}$ Fabs were injected over the trimer-bound surface to determine their affinities for BG505 SOSIP in its closed and open states. 8ANC195, 8ANC195$_{G52K5}$, and a chimeric Fab differing from 8ANC195 only in the K107R$_{HC}$ mutation (8ANC195$_{G52K5}$ HC/8ANC195 LC) bound to closed trimer with slightly higher affinities than to CD4-Fc-bound open trimer (Figures 4B and S3). No decrease in affinity was observed for 8ANC195$_{G52K5}$ binding to CD4-bound BG505 SOSIP captured by 17b or 21c, perhaps reflecting stabilization of the 8ANC195$_{G52K5}$-sCD4-BG505 SOSIP complex by the CD4-induced Abs.

We also attempted to determine a binding affinity for the interaction between 8ANC195 IgG-bound BG505 SOSIP trimers and sCD4. In reciprocal experiments to those described above, sCD4 was injected over 8ANC195-captured trimers. Only weak binding that could not be fit to a binding model was observed (Figure S3). Since sCD4 binds to unliganded BG505 SOSIP (Julien et al., 2013b) (Figures S1A and S1B), this result suggests that pre-binding of 8ANC195 to Env diminishes its ability to interact with CD4.

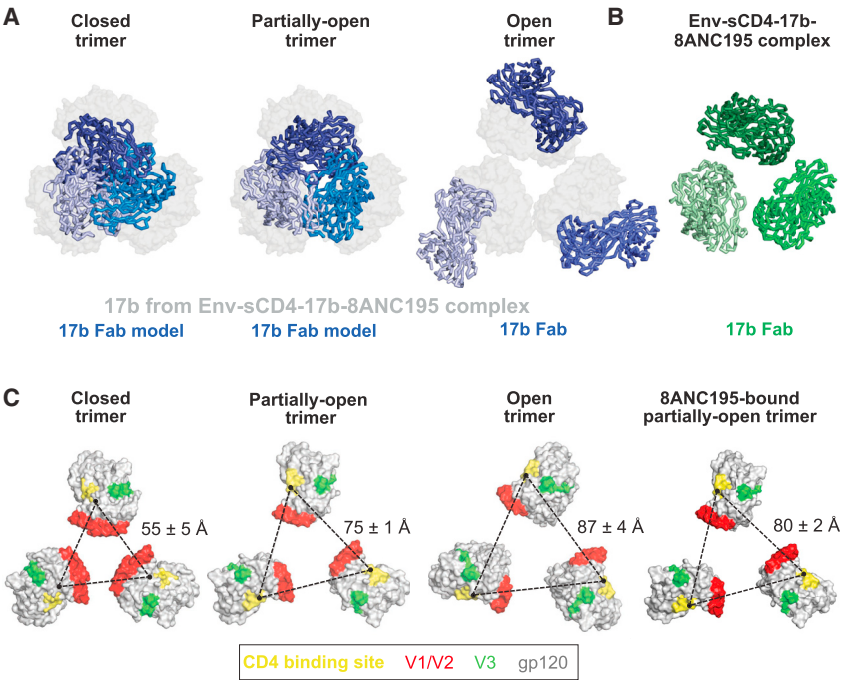

Figure 6. Comparison of Different Conformations of Env Trimers in BG505 SOSIP-sCD4-17b-8ANC195$_{G52K5}$ and Other Env Trimer Complexes Illustrated by 17b and gp120 Positions

(A) Overlay of 17b Fabs from BG505 SOSIP-sCD4-17b-8ANC195$_{G52K5}$ complex (gray space-filling representations) with 17b Fabs complexed with Env trimers in different conformational states (thick Cα traces in shades of blue). 17b Fabs shown after superimposition of gp120s from trimers (trimers and other ligands not shown). (Left) 17b modeled onto 3DNN coordinates of a closed trimer. (Middle) 17b modeled onto 3DNL coordinates of a partly open trimer. (Right) 17b taken from 3DNO structure of a CD4- and 17b-bound open trimer. Note that three 17b Fabs cannot be accommodated without clashes when modeled onto the gp120s of closed and partly open trimer structures.

(B) Cα trace of the three 17b Fabs from the BG505 SOSIP-sCD4-17b-8ANC195$_{G52K5}$ complex.

(C) Positions of gp120s (gray space-filling representation with locations of CD4-binding site in yellow, V3 loop in green, and base of V1V2 domain in red) in Env trimers adopting the indicated conformations. The locations of Asp368$_{gp120}$ are shown as a black dot for each trimer conformation, with the distance between the Cα of this residue in adjacent protomers indicated. Distances are presented as the mean and SD for the analogous distance in representative structures in each conformation.

See also Figure S6 and Table S5.

To verify and extend the structural details, we next determined a negative-stain single-particle reconstruction of the BG505 SOSIP-sCD4-17b-8ANC195$_{G52K5}$ complex at ~17 Å resolution (Figures 5B and S5). Potentially due to conditions during staining or drying of the grid or the low-sample concentrations necessary to obtain grids containing an optimal distribution of particles, not all complexes contained stoichiometric numbers of ligands. Therefore, we included a 3D classification procedure after reference-free 2D classification to sort particles containing the stoichiometric complex from sub-stoichiometric complexes, resulting in selection of approximately half of the initially selected particles from good 2D classes. The resulting reconstruction showed density for three copies each of 8ANC195$_{G52K5}$, 17b, and sCD4 bound to BG505 SOSIP, and we again fit the density using coordinates for gp120-sCD4-17b and 8ANC195 Fab structures (Figure 5B). The two reconstructions showed similar placements of three gp120s, three sCD4s, and six Fabs (Figures 5C). We used the higher-resolution single-particle reconstruction for subsequent analyses.

From comparisons with other Fab and Fab-sCD4-Env structures, it is evident that the trimer in our BG505 SOSIP-sCD4-17b-8ANC195$_{G52K5}$ structure is not in a closed conformation (Figure 6). As expected, given that the trimer is not closed, the placement of 8ANC195$_{G52K5}$ in the EM structure is shifted somewhat from its placement in the 8ANC195$_{G52K5}$-BG505 SOSIP (closed trimer) crystal structure (Figure S6). To determine whether the trimer in the EM structure is fully open, we investigated the arrangement of 17b Fabs, noting that they are positioned differently in the BG505 SOSIP-sCD4-17b-8ANC195$_{G52K5}$ structure than in open trimer structures (Figures 6A and 6B) (Harris et al., 2011; Liu et al., 2008; Sanders et al., 2013; Tran et al., 2012), suggesting that the trimer in the BG505 SOSIP-sCD4-17b-8ANC195$_{G52K5}$ complex is less open than in other sCD4-bound or 17b-bound structures. To more precisely describe the conformational state of the Env trimer in the BG505 SOSIP-sCD4-17b-8ANC195$_{G52K5}$ complex, we measured distances between a CD4bs residue in each gp120 protomer of the trimer and compared them to the corresponding distances in structures of trimers in different conformational states (Figures 1C and 6C and Table S5). This comparison showed that the trimer in the BG505 SOSIP-sCD4-17b-8ANC195$_{G52K5}$ structure adopts a previously unseen partially open state that is midway between a partially open state observed for Env bound to either b12 (a CD4bs Ab) or A12 VHH (a CD4bs llama Ab fragment) and the open state observed for the sCD4/17b-bound open trimer (Merk and Subramaniam, 2013). Thus, addition of 8ANC195$_{G52K5}$ Fab to the BG505 SOSIP-sCD4-17b complex resulted in partial closure of the trimer, suggesting that stable 8ANC195$_{G52K5}$ binding is incompatible with a fully open Env trimer conformation and would therefore block conformational changes leading to fusion between the viral and host membranes.

DISCUSSION

Here, we present an atomic resolution structure of 8ANC195$_{G52K5}$ bound to BG505 SOSIP, a native-like soluble HIV-1 Env trimer in the closed, prefusion conformation. The

interface of 8ANC195$_{G52K5}$ with Env trimer (5,645 Å^2 total buried surface area) is much larger than typical Ab-antigen complexes (Jones and Thornton, 1996), and 8ANC195 uses a large proportion of its accessible surface to engage its antigen, primarily using CDRs to contact protein portions and framework regions to contact glycan portions of the epitope. The structure solidifies previous evidence that the 8ANC195 epitope spans gp120 and gp41 (Scharf et al., 2014) and reveals details of extensive interactions with *N*-linked glycans on both gp120 and gp41. Rather than penetrating the glycan shield of HIV-1 Env with only a single loop, a strategy employed by Abs such as PG9 and PGT128 (McLellan et al., 2011; Pejchal et al., 2011), 8ANC195 inserts its entire variable region into a gap in the Env trimer glycan shield at the interface of gp120 and gp41. 8ANC195 makes productive interactions with gp120 glycans at Asn234$_{gp120}$ and Asn276$_{gp120}$, since neutralization potency decreases when these glycans are deleted (West et al., 2013). However, the mature Ab appears to accommodate, rather than productively contact, gp41 glycans, e.g., the Asn637$_{gp41}$ glycan, since the neutralization potency of 8ANC195 is not affected when this glycan is removed despite the large contact area between the Asn637$_{gp41}$ glycan and 8ANC195$_{G52K5}$.

In addition to recognizing both gp120 monomer and closed Env trimer, we also provide SPR and EM evidence that 8ANC195 can bind to Env trimers complexed with sCD4 and the CD4-induced Ab 17b. CD4 binding normally induces an open state of both virion-bound and soluble HIV-1 Env trimers involving rotation of gp120 subunits away from the center axis of the trimer (Harris et al., 2011; Liu et al., 2008; Sanders et al., 2013; Tran et al., 2012). However, despite recognizing an epitope that spans the gp120-gp41 interface, a region thought to undergo conformational changes upon CD4 binding to allow rotation of the gp120 subunits, 8ANC195 binds CD4-bound Env trimers with little to no decrease in affinity compared with closed, non-CD4-bound trimers. 17b, which binds at the apex of Env trimer, prevents reclosing of Env trimer that has opened upon CD4 binding because three 17b Fabs cannot be accommodated on a closed Env trimer (Figure 6A). Thus, our EM structure of a partially open BG505 SOSIP-sCD4-17b-8ANC195 complex suggests that 8ANC195 binding to fully open CD4-bound Env trimers results in a conformational change toward the closed state but that complete closure of the trimer is prevented by steric clashing of 17b Fabs. Alternatively, when Env trimer is bound to CD4, 8ANC195 could stabilize a partially open conformation in equilibrium with fully open CD4-bound Env. Taken together with our crystal structure showing a closed 8ANC195$_{G52K5}$-bound trimer despite pre-incubation of trimer with sCD4, the observation that the trimer in the BG505 SOSIP-sCD4-17b-8ANC195$_{G52K5}$ complex is partially, rather than fully, open implies that 8ANC195 prefers binding to the closed trimer. This suggests that its mechanism of neutralization likely involves preventing the complete conformational change necessary for the trimer to bind co-receptor and/or expose the fusion peptide and fuse with the target cell membrane.

Although our results suggest that 8ANC195 preferentially recognizes closed Env trimers, its ability to also recognize other Env conformations suggests that 8ANC195 can neutralize virions regardless of Env conformational state, including virions with constitutively open spikes such as those found on CD4-independent strains (White et al., 2010, 2011). It also suggests that, in addition to neutralizing free virions, 8ANC195 could neutralize virions already engaged by CD4 at a target cell membrane. This is a useful property of an HIV-1 bNAb since Abs with these properties could inhibit cell-to-cell spread of HIV-1, which is most effectively prevented by Abs that bind triggered Env conformations (Abela et al., 2012). Finally, recent evidence from single-molecule FRET studies (Munro et al., 2014) and molecular ruler measurements of virion-associated Env trimers (Galimidi et al., 2015) suggests that Env on free virions can exhibit transitions from the closed state to more open conformations; thus, recognition of Env states other than the closed state should be useful for neutralization of cell-bound as well as free virions.

The finding that the trimer in our BG505 SOSIP-sCD4-17b-8ANC195$_{G52K5}$ complex structure was partially, rather than fully, open, as observed in previous CD4-, 17b-, and CD4/17b-bound trimer structures (Harris et al., 2011; Liu et al., 2008; Sanders et al., 2013; Tran et al., 2012), suggests that the trimer re-closed somewhat upon 8ANC195 binding. This result implies more structural plasticity of HIV-1 Env than previously assumed and prompts reevaluation of current models for target cell fusion by Env after CD4 engagement to address, for example, whether the partially closed CD4-bound structure revealed in this work can engage co-receptors. We hypothesize that, when 8ANC195 engages a CD4-bound (open) trimer, it partially recloses the trimer or captures and stabilizes a pre-existing conformation because the complex with a partially open trimer is more favorable for Ab binding. This reclosing of the trimer may result in dissociation of CD4, either due to steric constraints on partially open trimers or the relatively low affinity of sCD4 for trimer (~600 nM) (Julien et al., 2013b). In stabilized soluble Env trimers, 8ANC195 binding may result in complete re-closure of the trimer, as observed in our BG505 SOSIP-8ANC195$_{G52K5}$ crystal structure. This model suggests that CD4 engagement of HIV-1 spike trimers does not lead to an immediate irreversible conformational change but, rather, that the conformational change is reversible as long as no major rearrangement of gp41 has occurred. Alternatively, the highly stabilized design of SOSIP trimers may be responsible for the apparent reversibility of CD4-induced conformational changes. However, single-molecule FRET experiments on HIV-1 virions showed that membrane-bound Env trimers sample three distinct conformational states in the absence of ligands and that ligands such as Abs and CD4 only changed the sizes of the populations occupying each state (Munro et al., 2014). The FRET study reported a sequence of conformational changes in unbound trimer involving transitions from closed to fully open, open to partially open, and then partially open to closed, supporting our hypothesis that membrane-bound Env trimers can re-close from a fully open state spontaneously, a process that may be assisted by an Ab that prefers to engage the closed state.

Combinations of bNAbs are being considered for treatment and prevention of HIV-1 infection by passive delivery methods because mixtures of active molecules (bNAbs or small molecule drugs) are required to prevent the appearance of escape mutants in a rapidly mutating virus such as HIV-1 (Horwitz et al., 2013; Klein et al., 2012). Two or more bNAbs targeting

different epitopes are favored because the virus is presumed unable to mutate several potentially conserved sites simultaneously. In addition to targeting an epitope distinct from other known bNAbs, 8ANC195 can accommodate different conformational states (including a CD4-bound state), making it an attractive candidate for use in combination therapies with bNAbs that (1) cannot tolerate such changes, (2) are unable to engage a CD4-bound open trimer, and/or (3) allow HIV-1 to spread through cell-to-cell transmission, as is the case for potent CD4-binding site Abs in the VRC01 family (Abela et al., 2012). 8ANC195 may also be a target for vaccine development since it targets conserved regions on Env such as gp41 and the Asn276$_{gp120}$ glycan.

EXPERIMENTAL PROCEDURES

Detailed methods are provided in the Supplemental Experimental Procedures.

Protein Production and Purification

8ANC195, 8ANC195$_{G52K5}$, 17b, PGT145, mG053, 2G12, CD4-Fc (domains 1 and 2 of human CD4 fused to human IgG1 Fc), human IgG1 Fc, and partially gl-reverted IgGs and/or Fabs were produced by transient transfection and purified using affinity and SEC, as described in previous studies (Diskin et al., 2011; Scharf et al., 2014). sCD4 (domains 1 and 2; residues 1–186 of mature CD4) was produced in baculovirus-infected Hi5 insect cells and was purified using affinity chromatography and SEC, as described previously (Diskin et al., 2010; Scharf et al., 2014). Untagged BG505 SOSIP.664 was constructed, expressed, and purified as described (Sanders et al., 2013). In brief, HEK293-6E cells treated with 5 μM kifunensine (Sigma) were co-transfected with plasmids encoding BG505 SOSIP.664 and soluble furin, and trimers were purified from cell supernatants using a 2G12 immunoaffinity chromatography and SEC.

Crystallization

Samples for crystallography were produced by incubating BG505 SOSIP with a 3-fold molar excess of sCD4 and were purified by SEC. The resulting complex was incubated with a 3-fold molar excess of 8ANC195$_{G52K5}$ Fab and purified by SEC. Crystals of 8ANC195$_{G52K5}$ Fab-BG505 SOSIP (space group $P2_1$; a = 117.74 Å, b = 195.22 Å, c = 119.09 Å; β = 101.6°) were obtained in 100 mM Tris (pH 8.0), 15% PEG 3,350, and 2% 1,4-dioxane at 20°C and frozen in liquid N_2 after cryoprotection.

Crystallographic Data Collection, Structure Determination, and Refinement

X-ray diffraction data were collected at the Argonne National Laboratory Advanced Photon Source (APS) beamline 23-ID-D using a MAR 300 CCD detector and were processed using XDS (Kabsch, 2010). The structure was solved by molecular replacement using a trimeric model of BG505 SOSIP (PDB: 4TVP) and three copies of 8ANC195 Fab (PDB: 4P9M). The model was refined to 3.58 Å using Phenix (Adams et al., 2010) and manual model building in Coot (Emsley and Cowtan, 2004). In the final model (R_{work} = 24.1%; R_{free} = 28.6%), 96%, 4%, and 0% of the residues were in the favored, allowed, and disallowed regions, respectively, of the Ramachandran plot.

SPR

Experiments were performed using a Biacore T200 (Biacore). Protein A coupled on a CM5 chip (Biacore) was used to immobilize capture proteins (PGT145 IgG, PGT121 IgG, CD4-Fc, 17b IgG, 21C IgG, or mG053 IgG control), followed by injection of human Fc to block remaining protein A binding sites. BG505 SOSIP was subsequently injected and washed with running buffer (HBS-EP+, GE Healthcare). 8ANC195, 8ANC195$_{G52K5}$, and mutant/chimeric Fabs were injected over flow cells at increasing concentrations (1.95 to 1,000 nM) at flow rates of 50 μl/min for 180 s and were allowed to dissociate for 600 s. Flow cells were regenerated with one pulse each of 10 mM glycine (pH 2.5) and 1 M guanidine HCl at a flow rate of 90 μl/min. On/off rates (k_a/k_d) and binding constants (K_Ds) were calculated by kinetic analyses after subtraction of backgrounds using a 1:1 binding model with or without a bulk reflective index (RI) correction as appropriate (Biacore T200 Evaluation software).

Cryoelectron Tomography

Purified BG505 SOSIP-sCD4-17b-8ANC195$_{G52K5}$ complexes were diluted to 60 μg/ml in TBS immediately before plunge freezing to avoid complex dissociation at low concentration. Quantifoil R2/2 NH2 copper finder grids were vitrified in liquid ethane using a Mark IV Vitrobot (FEI Company) and Tilt series (±60°, 1° angular increments) were collected on a FEI Tecnai G2 Polara transmission electron microscope equipped with 300 keV FEG, a Gatan energy filter, and a Gatan K2 Summit direct detector using the UCSF tomography software package (Zheng et al., 2007) under low-dose conditions (120 $e^-/Å^2$ total for the tilt series at ~8 μm underfocus) at a nominal magnification of 41,000× so that each pixel represented 2.6 Å. Tomographic reconstructions and CTF corrections were calculated using IMOD (Kremer et al., 1996). Subtomogram averaging of 1,745 subvolumes was performed using PEET (Nicastro et al., 2006) without an external reference or applying C3 symmetry, resulting in a ~23 Å structure estimated by a 0.143 gold-standard Fourier shell correlation (FSC) calculated using IMOD (Kremer et al., 1996).

Negative-Stain Single-Particle EM

Purified BG505 SOSIP-sCD4-17b-8ANC195$_{G52K5}$ complexes were diluted to 10 μg/ml in TBS immediately before adding 3 μl to a glow discharged ultrathin C film on holey carbon support film, 400 mesh, Cu grids (Ted Pella) followed by cross-linking using glutaraldehyde vapor and staining with uranyl acetate. Data were collected using a FEI Tecnai T12 transmission electron microscope operating at 120 keV equipped with a Gatan Ultrascan 2k × 2k CCD using a 0.5 s exposure time at a nominal magnification of 42,000× at 1 μm defocus, resulting in 2.5 Å per pixel. A total of 23,951 particles were picked using EMAN2.1 (Tang et al., 2007) and RELION (Scheres, 2012), and the CTF correction was done using EMAN2.1. Initial reference-free 2D class averaging was performed using RELION, and the particles were further sorted using 3D classification in RELION. Refinement was conducted using 80 Å low-pass-filtered structures calculated from models of 8ANC195-sCD4-17b docked onto gp120 cores of partially open (PDB: 3DNL) trimer and 7,174 particles with C3 symmetry applied. The resolution of the final reconstruction was ~17 Å calculated with RELION (Scheres, 2012) using a gold-standard FSC and a 0.143 cutoff, as recommended for resolution estimations for single-particle EM reconstructions (Scheres and Chen, 2012). Coordinates from crystal structures were fit into the sub-tomogram averaged or negative-stain single-particle EM structures using UCSF Chimera (Pettersen et al., 2004).

ACCESSION NUMBERS

Crystallographic atomic coordinates and structure factors were deposited in the Protein Data Bank under accession code PDB: 5CJX. EM reconstructions were deposited in the Electron Microscopy Data Bank under accession codes EMD: 3086 and EMD: 3096.

SUPPLEMENTAL INFORMATION

Supplemental Information includes Supplemental Experimental Procedures, six figures, and five tables and can be found with this article online at http://dx.doi.org/10.1016/j.cell.2015.08.035.

AUTHOR CONTRIBUTIONS

L.S. prepared samples for structural studies, solved and analyzed crystal structure, performed and analyzed binding studies, and analyzed neutralization and Ab mutant data; H.W., L.S., S.C. and A.W.M. collected EM data; H.W. and L.S. solved and analyzed EM structures; H.G. expressed and purified proteins; L.S., H.W., and P.J.B. analyzed data and wrote the manuscript.

ACKNOWLEDGMENTS

This research was supported by the National Institute Of Allergy and Infectious Diseases of the National Institutes of Health Grant HIVRAD P01 AI100148 (P.J.B.) (the content is solely the responsibility of the authors and does not necessarily represent the official views of the National Institutes of Health), the Bill and Melinda Gates Foundation (Collaboration for AIDS Vaccine Discovery Grant 1040753 [P.J.B.]), the National Institutes of Health Grant 2 P50 GM082545-06 (P.J.B.), the American Cancer Society Grant PF-13-076-01-MPC (L.S.), and the Molecular Observatory at Caltech supported by the Gordon and Betty Moore Foundation. We thank the Gordon and Betty Moore and Beckman Foundations for gifts to Caltech that helped support electron microscopy; Grant Jensen for advice and support for EM; Jost Vielmetter and the Caltech Protein Expression Center for producing proteins and use of the Biacore T200; Priyanthi Gnanapragasam and René Mares for performing neutralization assays; the beamline staff at the Advanced Photon Source GM/CA-CAT for use and support for beamline 23ID-D; Marta Murphy and Rachel Galimidi for assistance with figures; and Michel Nussenzweig, Johannes Scheid, and Anthony West for helpful discussions and critical reading of the manuscript.

Received: May 3, 2015
Revised: June 19, 2015
Accepted: July 28, 2015
Published: September 10, 2015

REFERENCES

Abela, I.A., Berlinger, L., Schanz, M., Reynell, L., Günthard, H.F., Rusert, P., and Trkola, A. (2012). Cell-cell transmission enables HIV-1 to evade inhibition by potent CD4bs directed antibodies. PLoS Pathog. *8*, e1002634.

Adams, P.D., Afonine, P.V., Bunkóczi, G., Chen, V.B., Davis, I.W., Echols, N., Headd, J.J., Hung, L.W., Kapral, G.J., Grosse-Kunstleve, R.W., et al. (2010). PHENIX: a comprehensive Python-based system for macromolecular structure solution. Acta Crystallogr. D Biol. Crystallogr. *66*, 213–221.

Binley, J.M., Ban, Y.E., Crooks, E.T., Eggink, D., Osawa, K., Schief, W.R., and Sanders, R.W. (2010). Role of complex carbohydrates in human immunodeficiency virus type 1 infection and resistance to antibody neutralization. J. Virol. *84*, 5637–5655.

Blattner, C., Lee, J.H., Sliepen, K., Derking, R., Falkowska, E., de la Peña, A.T., Cupo, A., Julien, J.P., van Gils, M., Lee, P.S., et al. (2014). Structural delineation of a quaternary, cleavage-dependent epitope at the gp41-gp120 interface on intact HIV-1 Env trimers. Immunity *40*, 669–680.

Capon, D.J., Chamow, S.M., Mordenti, J., Marsters, S.A., Gregory, T., Mitsuya, H., Byrn, R.A., Lucas, C., Wurm, F.M., Groopman, J.E., et al. (1989). Designing CD4 immunoadhesins for AIDS therapy. Nature *337*, 525–531.

Caskey, M., Klein, F., Lorenzi, J.C., Seaman, M.S., West, A.P., Jr., Buckley, N., Kremer, G., Nogueira, L., Braunschweig, M., Scheid, J.F., et al. (2015). Viraemia suppressed in HIV-1-infected humans by broadly neutralizing antibody 3BNC117. Nature *522*, 487–491.

Derking, R., Ozorowski, G., Sliepen, K., Yasmeen, A., Cupo, A., Torres, J.L., Julien, J.P., Lee, J.H., van Montfort, T., de Taeye, S.W., et al. (2015). Comprehensive antigenic map of a cleaved soluble HIV-1 envelope trimer. PLoS Pathog. *11*, e1004767.

Diskin, R., Marcovecchio, P.M., and Bjorkman, P.J. (2010). Structure of a clade C HIV-1 gp120 bound to CD4 and CD4-induced antibody reveals anti-CD4 polyreactivity. Nat. Struct. Mol. Biol. *17*, 608–613.

Diskin, R., Scheid, J.F., Marcovecchio, P.M., West, A.P., Jr., Klein, F., Gao, H., Gnanapragasam, P.N., Abadir, A., Seaman, M.S., Nussenzweig, M.C., and Bjorkman, P.J. (2011). Increasing the potency and breadth of an HIV antibody by using structure-based rational design. Science *334*, 1289–1293.

Elbein, A.D., Tropea, J.E., Mitchell, M., and Kaushal, G.P. (1990). Kifunensine, a potent inhibitor of the glycoprotein processing mannosidase I. J. Biol. Chem. *265*, 15599–15605.

Emsley, P., and Cowtan, K. (2004). Coot: model-building tools for molecular graphics. Acta Crystallogr. D Biol. Crystallogr. *60*, 2126–2132.

Galimidi, R.P., Klein, J.S., Politzer, M.S., Bai, S., Seaman, M.S., Nussenzweig, M.C., West, A.P., Jr., and Bjorkman, P.J. (2015). Intra-spike crosslinking overcomes antibody evasion by HIV-1. Cell *160*, 433–446.

Go, E.P., Hewawasam, G., Liao, H.X., Chen, H., Ping, L.H., Anderson, J.A., Hua, D.C., Haynes, B.F., and Desaire, H. (2011). Characterization of glycosylation profiles of HIV-1 transmitted/founder envelopes by mass spectrometry. J. Virol. *85*, 8270–8284.

Guttman, M., Cupo, A., Julien, J.P., Sanders, R.W., Wilson, I.A., Moore, J.P., and Lee, K.K. (2015). Antibody potency relates to the ability to recognize the closed, pre-fusion form of HIV Env. Nat. Commun. *6*, 6144.

Harris, A., Borgnia, M.J., Shi, D., Bartesaghi, A., He, H., Pejchal, R., Kang, Y.K., Depetris, R., Marozsan, A.J., Sanders, R.W., et al. (2011). Trimeric HIV-1 glycoprotein gp140 immunogens and native HIV-1 envelope glycoproteins display the same closed and open quaternary molecular architectures. Proc. Natl. Acad. Sci. USA *108*, 11440–11445.

Horwitz, J.A., Halper-Stromberg, A., Mouquet, H., Gitlin, A.D., Tretiakova, A., Eisenreich, T.R., Malbec, M., Gravemann, S., Billerbeck, E., Dorner, M., et al. (2013). HIV-1 suppression and durable control by combining single broadly neutralizing antibodies and antiretroviral drugs in humanized mice. Proc. Natl. Acad. Sci. USA *110*, 16538–16543.

Huang, J., Kang, B.H., Pancera, M., Lee, J.H., Tong, T., Feng, Y., Imamichi, H., Georgiev, I.S., Chuang, G.Y., Druz, A., et al. (2014). Broad and potent HIV-1 neutralization by a human antibody that binds the gp41-gp120 interface. Nature *515*, 138–142.

Jones, S., and Thornton, J.M. (1996). Principles of protein-protein interactions. Proc. Natl. Acad. Sci. USA *93*, 13–20.

Julien, J.P., Cupo, A., Sok, D., Stanfield, R.L., Lyumkis, D., Deller, M.C., Klasse, P.J., Burton, D.R., Sanders, R.W., Moore, J.P., et al. (2013a). Crystal structure of a soluble cleaved HIV-1 envelope trimer. Science *342*, 1477–1483.

Julien, J.P., Sok, D., Khayat, R., Lee, J.H., Doores, K.J., Walker, L.M., Ramos, A., Diwanji, D.C., Pejchal, R., Cupo, A., et al. (2013b). Broadly neutralizing antibody PGT121 allosterically modulates CD4 binding via recognition of the HIV-1 gp120 V3 base and multiple surrounding glycans. PLoS Pathog. *9*, e1003342.

Kabsch, W. (2010). Integration, scaling, space-group assignment and post-refinement. Acta Crystallogr. D Biol. Crystallogr. *66*, 133–144.

Klein, F., Halper-Stromberg, A., Horwitz, J.A., Gruell, H., Scheid, J.F., Bournazos, S., Mouquet, H., Spatz, L.A., Diskin, R., Abadir, A., et al. (2012). HIV therapy by a combination of broadly neutralizing antibodies in humanized mice. Nature *492*, 118–122.

Kremer, J.R., Mastronarde, D.N., and McIntosh, J.R. (1996). Computer visualization of three-dimensional image data using IMOD. J. Struct. Biol. *116*, 71–76.

Kwon, Y.D., Finzi, A., Wu, X., Dogo-Isonagie, C., Lee, L.K., Moore, L.R., Schmidt, S.D., Stuckey, J., Yang, Y., Zhou, T., et al. (2012). Unliganded HIV-1 gp120 core structures assume the CD4-bound conformation with regulation by quaternary interactions and variable loops. Proc. Natl. Acad. Sci. USA *109*, 5663–5668.

Do Kwon, Y., Pancera, M., Acharya, P., Georgiev, I.S., Crooks, E.T., Gorman, J., Joyce, M.G., Guttman, M., Ma, X., Narpala, S., et al. (2015). Crystal structure, conformational fixation and entry-related interactions of mature ligand-free HIV-1 Env. Nat. Struct. Mol. Biol. *22*, 522–531.

Liu, J., Bartesaghi, A., Borgnia, M.J., Sapiro, G., and Subramaniam, S. (2008). Molecular architecture of native HIV-1 gp120 trimers. Nature *455*, 109–113.

Lyumkis, D., Julien, J.P., de Val, N., Cupo, A., Potter, C.S., Klasse, P.J., Burton, D.R., Sanders, R.W., Moore, J.P., Carragher, B., et al. (2013). Cryo-EM structure of a fully glycosylated soluble cleaved HIV-1 envelope trimer. Science *342*, 1484–1490.

McLellan, J.S., Pancera, M., Carrico, C., Gorman, J., Julien, J.P., Khayat, R., Louder, R., Pejchal, R., Sastry, M., Dai, K., et al. (2011). Structure of HIV-1 gp120 V1/V2 domain with broadly neutralizing antibody PG9. Nature *480*, 336–343.

Merk, A., and Subramaniam, S. (2013). HIV-1 envelope glycoprotein structure. Curr. Opin. Struct. Biol. *23*, 268–276.

Mouquet, H., Scharf, L., Euler, Z., Liu, Y., Eden, C., Scheid, J.F., Halper-Stromberg, A., Gnanapragasam, P.N., Spencer, D.I., Seaman, M.S., et al. (2012). Complex-type N-glycan recognition by potent broadly neutralizing HIV antibodies. Proc. Natl. Acad. Sci. USA *109*, E3268–E3277.

Munro, J.B., Gorman, J., Ma, X., Zhou, Z., Arthos, J., Burton, D.R., Koff, W.C., Courter, J.R., Smith, A.B., 3rd, Kwong, P.D., et al. (2014). Conformational dynamics of single HIV-1 envelope trimers on the surface of native virions. Science *346*, 759–763.

Nicastro, D., Schwartz, C., Pierson, J., Gaudette, R., Porter, M.E., and McIntosh, J.R. (2006). The molecular architecture of axonemes revealed by cryoelectron tomography. Science *313*, 944–948.

Pancera, M., Zhou, T., Druz, A., Georgiev, I.S., Soto, C., Gorman, J., Huang, J., Acharya, P., Chuang, G.Y., Ofek, G., et al. (2014). Structure and immune recognition of trimeric pre-fusion HIV-1 Env. Nature *514*, 455–461.

Pejchal, R., Doores, K.J., Walker, L.M., Khayat, R., Huang, P.S., Wang, S.K., Stanfield, R.L., Julien, J.P., Ramos, A., Crispin, M., et al. (2011). A potent and broad neutralizing antibody recognizes and penetrates the HIV glycan shield. Science *334*, 1097–1103.

Pettersen, E.F., Goddard, T.D., Huang, C.C., Couch, G.S., Greenblatt, D.M., Meng, E.C., and Ferrin, T.E. (2004). UCSF Chimera–a visualization system for exploratory research and analysis. J. Comput. Chem. *25*, 1605–1612.

Pugach, P., Ozorowski, G., Cupo, A., Ringe, R., Yasmeen, A., de Val, N., Derking, R., Kim, H.J., Korzun, J., Golabek, M., et al. (2015). A native-like SOSIP.664 trimer based on an HIV-1 subtype B env gene. J. Virol. *89*, 3380–3395.

Sanders, R.W., Derking, R., Cupo, A., Julien, J.P., Yasmeen, A., de Val, N., Kim, H.J., Blattner, C., de la Peña, A.T., Korzun, J., et al. (2013). A next-generation cleaved, soluble HIV-1 Env trimer, BG505 SOSIP.664 gp140, expresses multiple epitopes for broadly neutralizing but not non-neutralizing antibodies. PLoS Pathog. *9*, e1003618.

Scharf, L., Scheid, J.F., Lee, J.H., West, A.P., Jr., Chen, C., Gao, H., Gnanapragasam, P.N., Mares, R., Seaman, M.S., Ward, A.B., et al. (2014). Antibody 8ANC195 reveals a site of broad vulnerability on the HIV-1 envelope spike. Cell Rep. *7*, 785–795.

Scheid, J.F., Mouquet, H., Ueberheide, B., Diskin, R., Klein, F., Oliveira, T.Y., Pietzsch, J., Fenyo, D., Abadir, A., Velinzon, K., et al. (2011). Sequence and structural convergence of broad and potent HIV antibodies that mimic CD4 binding. Science *333*, 1633–1637.

Scheres, S.H. (2012). RELION: implementation of a Bayesian approach to cryo-EM structure determination. J. Struct. Biol. *180*, 519–530.

Scheres, S.H., and Chen, S. (2012). Prevention of overfitting in cryo-EM structure determination. Nat. Methods *9*, 853–854.

Sullivan, N., Sun, Y., Sattentau, Q., Thali, M., Wu, D., Denisova, G., Gershoni, J., Robinson, J., Moore, J., and Sodroski, J. (1998). CD4-Induced conformational changes in the human immunodeficiency virus type 1 gp120 glycoprotein: consequences for virus entry and neutralization. J. Virol. *72*, 4694–4703.

Tang, G., Peng, L., Baldwin, P.R., Mann, D.S., Jiang, W., Rees, I., and Ludtke, S.J. (2007). EMAN2: an extensible image processing suite for electron microscopy. J. Struct. Biol. *157*, 38–46.

Tran, E.E., Borgnia, M.J., Kuybeda, O., Schauder, D.M., Bartesaghi, A., Frank, G.A., Sapiro, G., Milne, J.L., and Subramaniam, S. (2012). Structural mechanism of trimeric HIV-1 envelope glycoprotein activation. PLoS Pathog. *8*, e1002797.

West, A.P., Jr., Scharf, L., Horwitz, J., Klein, F., Nussenzweig, M.C., and Bjorkman, P.J. (2013). Computational analysis of anti-HIV-1 antibody neutralization panel data to identify potential functional epitope residues. Proc. Natl. Acad. Sci. USA *110*, 10598–10603.

West, A.P., Jr., Scharf, L., Scheid, J.F., Klein, F., Bjorkman, P.J., and Nussenzweig, M.C. (2014). Structural insights on the role of antibodies in HIV-1 vaccine and therapy. Cell *156*, 633–648.

White, T.A., Bartesaghi, A., Borgnia, M.J., Meyerson, J.R., de la Cruz, M.J., Bess, J.W., Nandwani, R., Hoxie, J.A., Lifson, J.D., Milne, J.L., and Subramaniam, S. (2010). Molecular architectures of trimeric SIV and HIV-1 envelope glycoproteins on intact viruses: strain-dependent variation in quaternary structure. PLoS Pathog. *6*, e1001249.

White, T.A., Bartesaghi, A., Borgnia, M.J., de la Cruz, M.J., Nandwani, R., Hoxie, J.A., Bess, J.W., Lifson, J.D., Milne, J.L., and Subramaniam, S. (2011). Three-dimensional structures of soluble CD4-bound states of trimeric simian immunodeficiency virus envelope glycoproteins determined by using cryo-electron tomography. J. Virol. *85*, 12114–12123.

Xiang, S.H., Doka, N., Choudhary, R.K., Sodroski, J., and Robinson, J.E. (2002). Characterization of CD4-induced epitopes on the HIV type 1 gp120 envelope glycoprotein recognized by neutralizing human monoclonal antibodies. AIDS Res. Hum. Retroviruses *18*, 1207–1217.

Zheng, S.Q., Keszthelyi, B., Branlund, E., Lyle, J.M., Braunfeld, M.B., Sedat, J.W., and Agard, D.A. (2007). UCSF tomography: an integrated software suite for real-time electron microscopic tomographic data collection, alignment, and reconstruction. J. Struct. Biol. *157*, 138–147.